Improvements in Flight Table Dynamic Transparency for Hardware-In-The-Loop Facilities

Louis A. DeMore[a], Paul R. Mackin[b], Michael Swamp[a], Roger Rusterholtz[c]

[a] Acutronic USA Inc, 139 Delta Drive, Pittsburgh Pennsylvania 15238
[b] AFRL/MNGG 101 West Eglin Blvd, Suite 234, Eglin AFB, Florida 32542
[c] Acutronic (Schweiz) AG, Techcenter Schwarz 8608 Bubicon, Switzerland

Abstract

Flight tables are a "necessary evil" in the Hardware-In-The-Loop (HWIL) simulation. Adding the actual or prototypic flight hardware to the loop, in order to increase the realism of the simulation, forces us to add motion simulation to the process. Flight table motion bases bring unwanted dynamics, non-lineariaties, transport delays, etc to an already difficult problem sometimes requiring the simulation engineer to compromise the results. We desire that the flight tables be "dynamically transparent" to the simulation scenario. This paper presents a State Variable Feedback (SVF) control system architecture with feed-forward techniques that improves the flight table's dynamic transparency by significantly reducing the table's low frequency phase lag. We offer some actual results with existing flight tables that demonstrate the improved transparency. These results come from a demonstration conducted on a flight table in the KHILS laboratory at Eglin AFB and during a refurbishment of a flight table for the Boeing Company of St. Charles, Missouri.

Keywords: flight tables, feed-forward, SVF control

1. Introduction

The HWIL test and simulation laboratory combines physical effect simulators with computers operating in real time. The physical effect simulators generally consist of:

- a three-axis table that simulates the roll, pitch and yaw of the missile motion
- a two-axis table that simulates the azimuth and elevation of the target Line-of-Sight(LOS) angle, and
- a target scene generator that simulates the target image in the required wavelengths.

The three and two axes flight tables in the HWIL laboratory must appear "transparent" with respect to the dynamic behavior of the missile-target engagement scenario in order to produce a high fidelity simulation. The motion simulators must produce motion that has minimal phase lag and gain attenuation over the frequency band of interest and also exhibit minimal non-linear motion for large signal commands.

From [1], we can reproduce a simple illustration of the effect that the flight table dynamics have on the overall HWIL simulation. Consider the two-dimensional air-to-ground engagement geometry shown in figure 1-1.

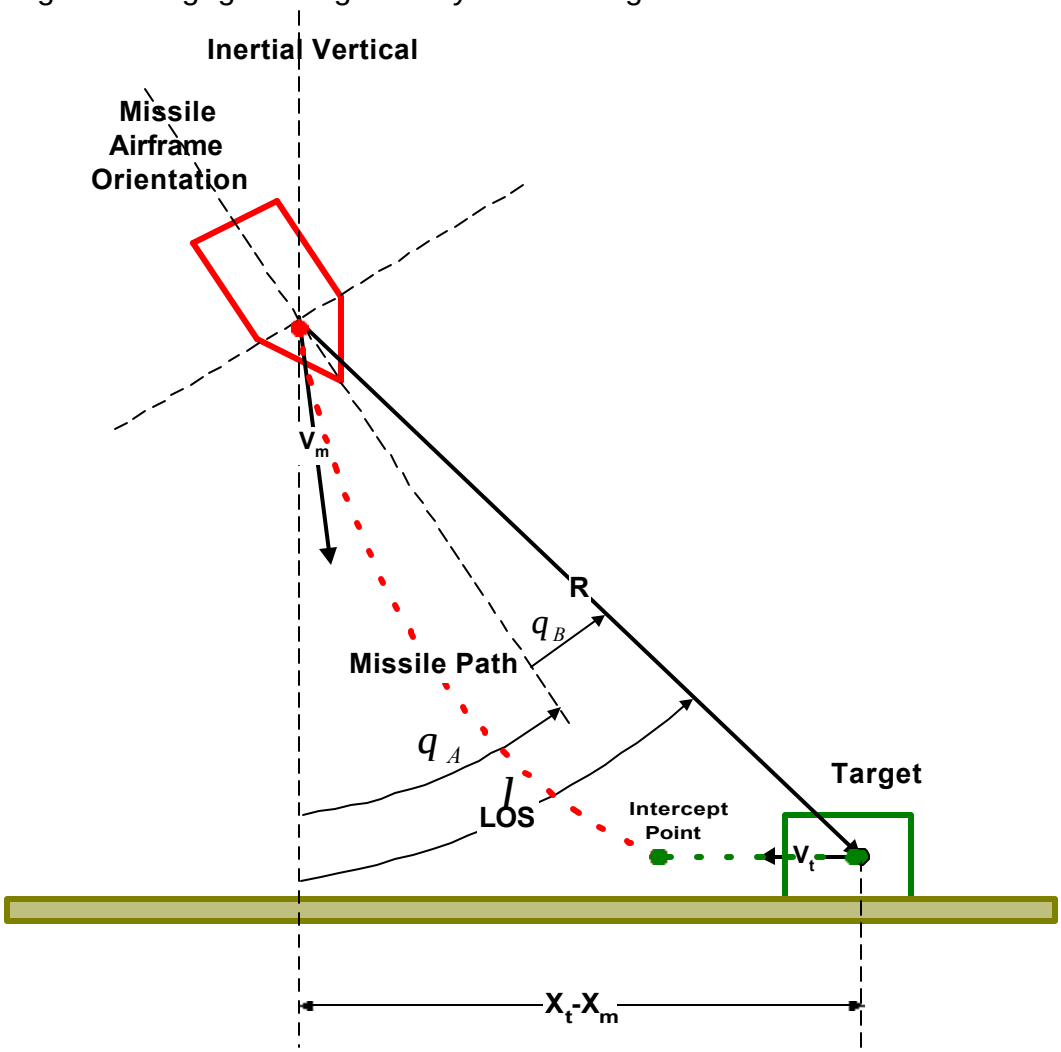

Figure 1-1 Two Dimensional Missile-to-Target Engagement Scenario Showing the Overall Engagement Geometry and the Missile Body Orientation During the Engagement

In the figure, if we just simply consider the missile and target as points with no body orientation then we create the overall engagement geometry. From the figure the overall engagement geometry contains the following variables:

$l \cong$ *Line-of-Site (LOS) angle, from missile to target*

$X_m \cong$ *missile position*

$X_t \cong$ *target position*

$R \cong$ *range vector from missile to target* ,

$V_m \cong$ *missile velocity vector*

$V_t \cong$ *target velocity vector*

The LOS angle, l, is the angle between the inertial vertical and the range vector, R. Both l and R vary as the engagement plays out. The relationship between l and R, for small l, is simply:

$$\sin(l) = \frac{X_m - X_t}{|R|} \approx l$$

Figure 1-1 also shows the body orientation of the missile during the engagement with the target.

We can see in the figure how the variables related to the missile airframe orientation relate to the overall engagement geometry variables. The additional missile orientation variables shown in the figure are:

$q_A \cong$ *airframe orientation w.r.t. inertial vertical*

$q_B \cong$ *missile seeker boresight error angle*

We assume that a target seeker is onboard the missile that generates a boresight error angle, q_B, between the missile airframe and the target. We can measure the airframe orientation angle, q_A, with a strapped down gyro on the missile body or as a part of the seeker. We write the relationship for q_B, q_A and l as:

$$l = q_A + q_B$$

Figure 1-2 is a simplified block diagram of the two-dimensional engagement problem showing the overall missile-to-target engagement geometry and the missile body orientation. The figure contains a missile seeker and autopilot and uses a proportional navigation tracking algorithm.

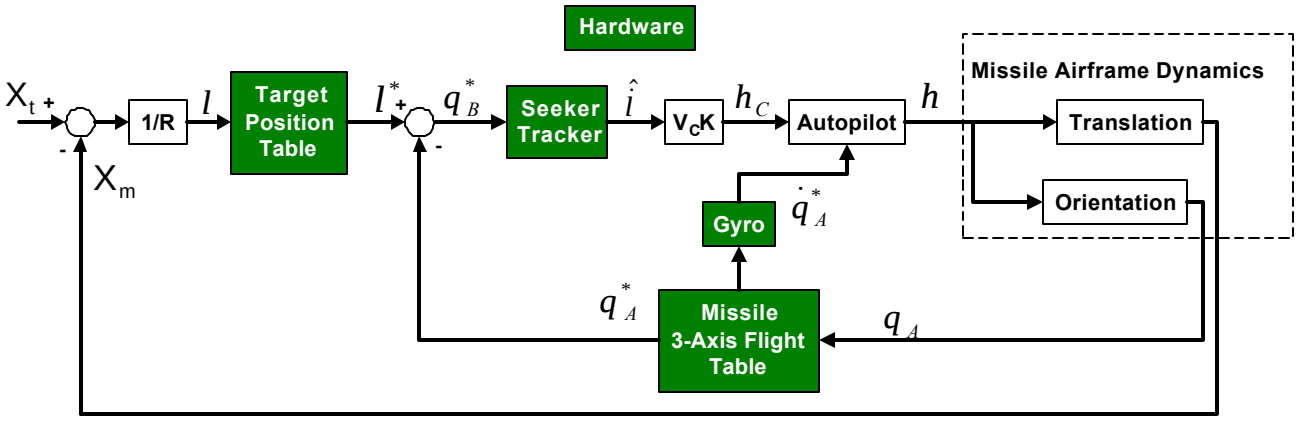

Figure 1-2 Simplified Block Diagram of Two-Dimensional Missile/Target Engagement

The additional variables in figure 1-2 are:

$l^* \cong$ *simulated LOS Angle*

$\hat{\dot{l}} \cong$ *LOS angular rate estimate*

$q^*_A \cong$ *simulated airframe orientation angle*

$q^*_B \cong$ *simulated seeker boresight error angle*

$V_C \cong$ *closing velocity*

$h_C \cong$ *normal acceleration command to missile*

The missile seeker/tracker generates the LOS angular rate estimate, $\hat{\dot{l}}$. The proportional navigator produces the normal acceleration command, h_C, to the missile autopilot that is proportional to the closing velocity, V_C, and $\hat{\dot{l}}$. The figure also shows the interfaces between the hardware (physical effects) and the software (simulation computer) elements of the simulation laboratory. The variables l^* and q^*_A are the missile flight table's and target motion table's responses to commands l and q_A.

The hardware elements in the figure are shaded and consist of:

- target position table
- missile flight table
- missile seeker and tracker
- body rate gyro

The scenario defined by figure 1-2 can also be played out totally with a simulation computer. We can run the simulation in either real time or non-real time to compute the "miss distance" for various models of the target, missile, seeker, etc. We increase the realism of the simulation by adding some of the flight hardware to the simulation; e.g. the missile seeker and the body rate gyro. Adding the flight hardware also requires the three-axis missile flight table to

simulate the missile body orientation and the two-axis target position table to simulate the missile-to-target LOS.

The figure shows the significant effect that the target position table and missile flight table will have on the overall fidelity of the simulation and demonstrates the need for transparency. Any motion table dynamic lag or non-linearity will compromise the simulation. From an input/output transfer function standpoint we desire the flight table to have unity gain and zero degrees phase lag for all frequencies to be perfectly transparent. However, we will settle for minimum phase lag and gain attenuation over the frequency band of interest. Usually this is 10 Hz and below for the three-axis table in the inner autopilot loop and 1 Hz and below for the two-axis table in the outer missile-target engagement loop.

In the following sections of this paper we demonstrate the ability our SVF, digital control (the Acutrol®) to increase dynamic transparency of the flight table. The Acutrol axis servo system architecture includes a State Observer and a State Variable Feedback control, an internal pressure feedback servo and a command generator.

2. Flight Table Servo Characteristics

In many cases the servo system is almost an afterthought during the design of the flight motion table. This often leads to mediocre performance of the axis servo systems. A design approach that requires the servo and mechanical designers to work concurrently is best. This systematic approach forces the designers to view the physical plant in terms of its servo dynamics. We produce design requirements (or trade-offs) for the mechanical plant by first creating a plant model based on an idealistic view of the flight table dynamics. From the assumptions underlying this idealistic model we can then assert mechanical design requirements. A compromise between the servo designer's desires and the mechanical design's practical constraints produce the optimal results.

For the hydraulic flight table a convenient set of system states for our "ideal" plant are position (q), rate ($\dot{q}$) and the actuator differential pressure (Δp). With this state representation we can describe the rigid body modes as well as the hydraulic compliance; but we ignore the structure's flexible body modes and the servo valve's second order dynamics. This results in a third order linear system:

$$\begin{bmatrix} \Delta\dot{p} \\ \ddot{q} \\ \dot{q} \end{bmatrix} = \begin{bmatrix} -\frac{1}{t} & -\frac{D}{Lt} & 0 \\ \frac{D}{J} & 0 & 0 \\ 0 & 1 & 0 \end{bmatrix} \begin{bmatrix} \Delta p \\ \dot{q} \\ q \end{bmatrix} + \begin{bmatrix} \frac{1}{Lt} \\ 0 \\ 0 \end{bmatrix} q$$

$$q \equiv servo\ valve\ flow$$

$$t \equiv \left(\frac{4b}{V}\right)L \equiv Hydraulic\ Time\ Constant$$

$$L \equiv Hydraulic\ Actuator\ Cross\text{-}Port\ Leakage$$

where: $V \equiv Hydraulic\ Trapped\ Volume$

$$b \equiv Bulk\ Modulus\ of\ Oil$$

$$D \equiv\ Actuator\ Displacement$$

$$J \equiv\ Rotating\ Inertia$$

We must balance our desire for the ideal flight table (a third order linear system) with the reality of the high order, non-linear physical plant. Our compromise is to maximize the linear operating region by making appropriate design choices during the mechanical/hydraulic design effort. The trade-off exercise results in the following design requirements:

- Separate the frequency domain location of the hydraulic resonance from the location of the servo valve dynamics
- Use fast response servo valves
- Keep the lowest torsional structural mode well beyond the servo crossover frequency
- Minimize actuator break-away friction and optimize actuator leakage

These design assumptions in allow us to design a pressure control inner-loop with a bandwidth well in excess of the hydraulic resonance frequency.

The high pass pressure loop effectively de-couples the hydraulic plant from the mechanical body dynamics. Figure 2-1 shows the pressure control system with the hydro-mechanical plant including the flexible structure.

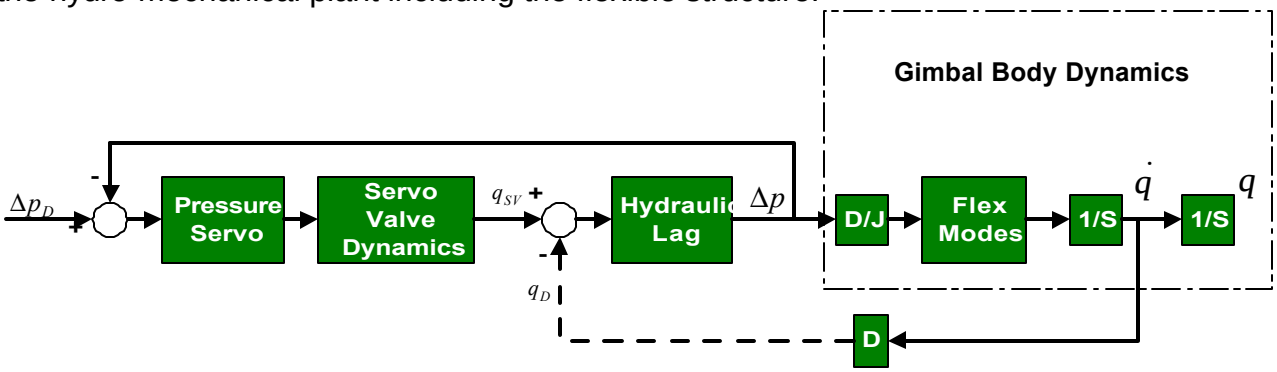

Figure 2-1 Pressure Servo Loop Showing the Hydro-Mechanical Plant with the Flexible Structure and the Mechanical Feedback Path (dashed)

The wide bandwidth pressure loop reacts to the mechanical feedback path, shown as dashed in the figure, as a servo disturbance. The control system will attempt to reject the effects of this path and essentially de-couple the hydraulic forward path from the mechanical feedback path. The result is a benign residual of the mechanical dynamics including the flexible dynamics.

We can now describe the system as two (de-coupled) cascaded second order systems. We add an augmented state variable representing the control integrator, i.e.

$$\dot{q} = u = k\left(\Delta p_D - \Delta p\right)$$

Ignoring the flexible modes again, this is :

$$\begin{bmatrix} \dot{q} \\ \Delta\dot{p} \end{bmatrix} = \begin{bmatrix} 0 & -k \\ \dfrac{1}{tL} & -\dfrac{1}{t} \end{bmatrix} \begin{bmatrix} q \\ \Delta p \end{bmatrix} + \begin{bmatrix} k \\ 0 \end{bmatrix} \Delta p_D \ , \ y_1 = \begin{bmatrix} 0 & \dfrac{D}{J} \end{bmatrix} \begin{bmatrix} q \\ \Delta p \end{bmatrix}$$

$$\begin{bmatrix} \ddot{q} \\ \dot{q} \end{bmatrix} = \begin{bmatrix} 0 & 0 \\ 1 & 0 \end{bmatrix} \begin{bmatrix} \dot{q} \\ q \end{bmatrix} + \begin{bmatrix} 1 \\ 0 \end{bmatrix} y_1 \ , \ y_2 = \begin{bmatrix} 0 & 1 \end{bmatrix} \begin{bmatrix} \dot{q} \\ q \end{bmatrix}$$

where: $\Delta p_D \equiv$ *presure control demand*

A very good example of a hydraulic flight table designed for enhanced servo performance is the Acutronic model HD756. We are building the table for DASA in Germany to be used as part of a HWIL missile test laboratory. Figure 2-2 is a photograph of the flight table during final mechanical assembly at our facility in Switzerland.

Figure 2-2 The Model HD756 Hydraulic Flight Table in Final Assembly

The figure shows the two-axis target gimbal set and the three-axis missile gimbal set of the flight table. The system is completely assembled with all hydraulic actuators and servo components in place.

3. Digital Control System Architecture

Our SVF architecture provides feedback control for the system states q, $\dot{q}$ and Δp; this architecture produces two very important control system features. The first feature is the ability to place the closed loop poles at desirable locations, which optimizes both transient performance and stability margins. The second feature is the ability of the control system to accept feed-forward commands to the individual state servo loops. We use these feed-forward techniques to reduce the apparent closed loop phase lag in the low frequency band below the position loop bandwidth. Applying feed-forward changes the closed loop transfer function from the original closed loop transfer function, i.e.:

$$\left(\frac{dq}{dq_C}\right)_W = G_{FF}(s)\left(\frac{dq}{dq_C}\right)_{W/O}$$

where:

$$\left(\frac{dq}{dq_C}\right)_W \equiv transfer\ function\ With\ feed\text{-}forward$$

$$G_{FF}(s) \equiv feed-forward\ transfer function$$

$$\left(\frac{dq}{dq_C}\right)_{W/O} \equiv transfer\ function\ Without\ feed\text{-}forward$$

As an example, the rate feed-forward lead term is given by:

$$G_{FF}(s)_{rate} = 1 + \frac{s}{w_p}$$

where w_p is the position loop crossover frequency.

Rate feed-forward alone will reduce the phase lag of a 20 Hz, 0.7 damped second order system from 25 degrees to 8 degrees at 6 Hz. The resulting 20 Hz, 0.7 damped system with rate feed-forward will have ½ the phase lag of a 30 Hz, 0.7 damped system at 6 Hz. The actual results from applying feed-forward techniques will be limited by the physical constraints of the system. The feed-forward architecture requires computation of the complete feed-forward command vector during each of the host computer's sample interval. If the host computer cannot generate the complete vector during each interval then the digital control system's command generator must construct the missing states from past data.

Figure 3-1 shows the control system architecture that we will use to servo our model HD756 hydraulic flight table and that we used in our demonstration at the AFWRL KHILS laboratory and in our flight table refurbishment for the Boeing Company.

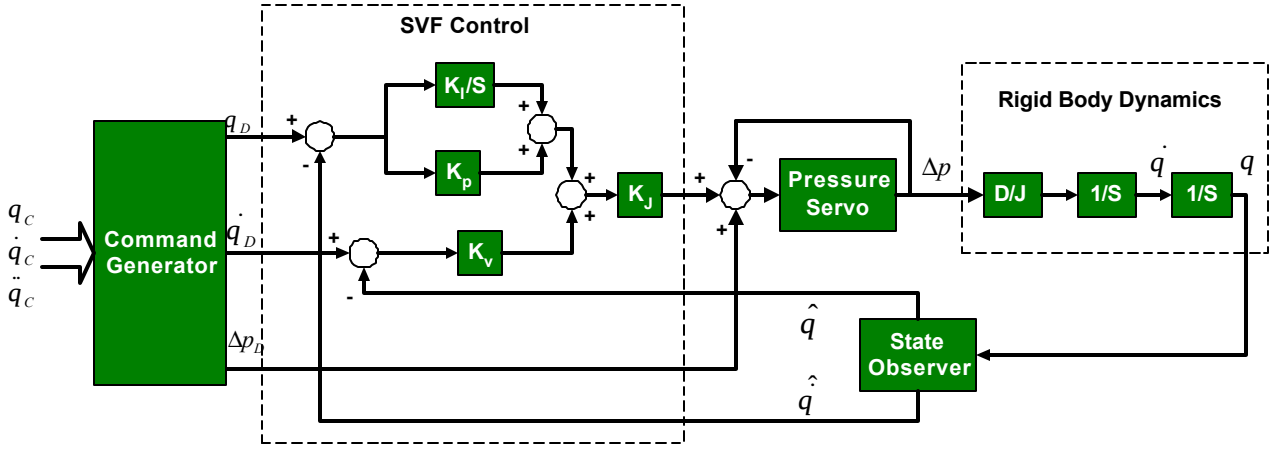

Figure 3-1 Control System Architecture Showing Interconnection of the Servo System Elements and the Physical Plant

The figure shows the state observer producing the rigid body states, the pressure feedback servo sub-loop, the SVF rigid body controller, and the state vector command generator with feed-forward commands.

4.Performance Data

We have two cases that clearly demonstrate the ability of the SVF digital control to reduce the low frequency phase lag and thereby improve the dynamic transparency of the flight table. The first case was a demonstration conducted in the KHILS laboratory at Eglin AFB. Here we replaced the flight table's existing outer axis analog position servo with the Digital SVF control system described in section 3. In the second case we replaced all three axes controllers of the flight table with our digital SVF control system. We completed this latter work as part of a contract with the Boeing Company of St. Charles Mo. In both cases the primary improvement was increased servo bandwidth characterized by a reduction of the closed loop phase lag at and below 10 Hz.

4.1 KHILS Demonstration

The KHILS flight table is site reconfigurable for either limited gimbal travel, high bandwidth operation or larger gimbal travel at lower bandwidths. For this demonstration the table was in its larger travel-lower bandwidth configuration. Figure 4-1 is the original closed loop frequency response of the flight table's outer axis position servo.

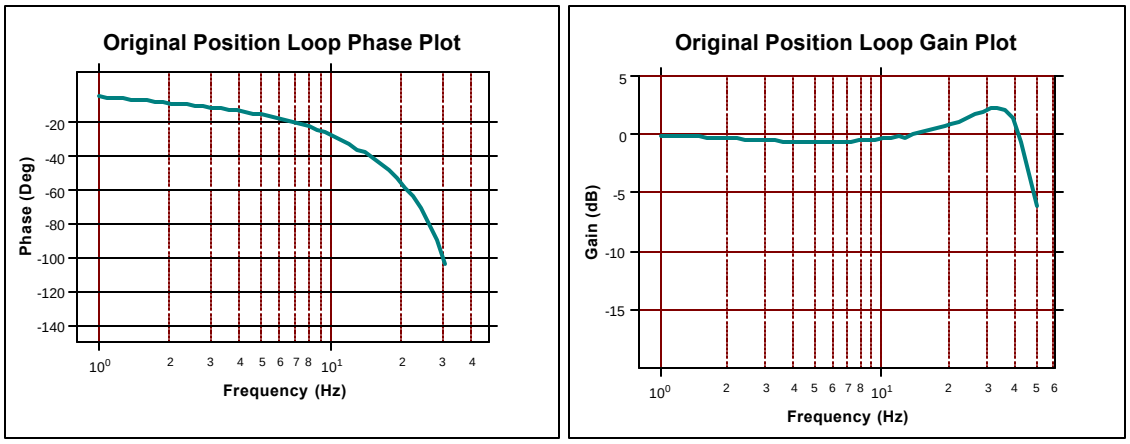

Figure 4-1 Outer Axis Original Closed Loop Frequency Response Showing a Phase Lag of 28 Degrees at 10 Hz

The original frequency data shows the outer axis to have a bandwidth (frequency at 90-degree phase lag) of 29 Hz with a 10 Hz phase lag of 28 degrees. For the demonstration, we completely removed the existing outer axis controller and replaced it with our digital SVF controller. The axis had only one pressure transducer measuring differential pressure across one of the axis dual vane actuators so we added another pressure transducer to measure differential pressure across the other dual vane actuator. The pressure servo consists of a single compensator driving both actuator servo valves and using the average of the two actuator differential pressures as the feedback variable. Figure 4-2 shows the closed loop frequency response for the cascaded pressure loop.

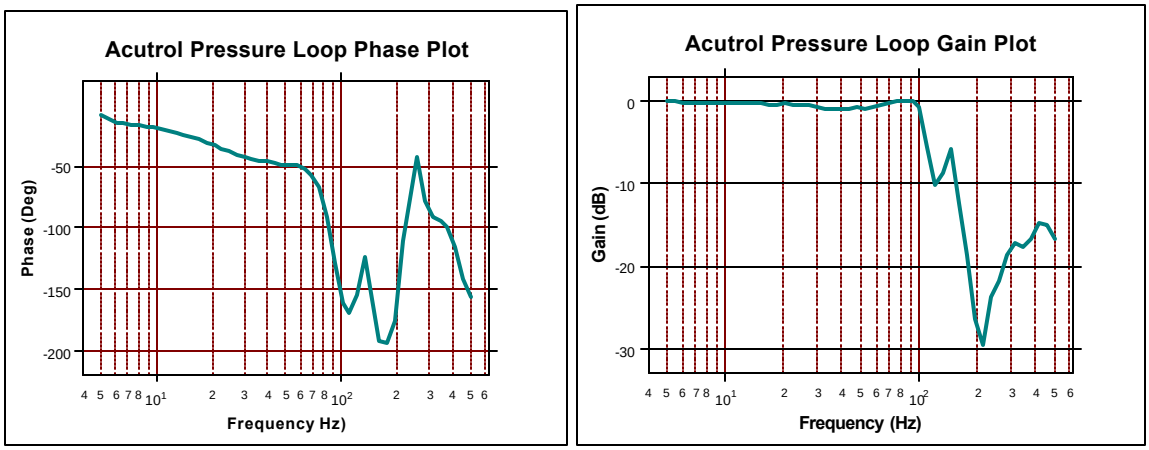

Figure 4-2 Pressure Servo Closed Loop Frequency Response Showing a Bandwidth (Frequency at 90 Degree Phase Lag) of 84 Hz

The pressure loop bandwidth of 84 Hz is about an octave above the axis hydraulic resonance. This is a very important and significant characteristic of our SVF control architecture. While the original axis control system limits itself to a position loop bandwidth well below the hydraulic resonance; the SVF control loop bandwidth is limited only by the structural resonance. Consequently, the SVF

controller has an inherent advantage in producing wider bandwidth axis control systems. Additionally, the pressure loop provides the necessary servo to accept the pressure feed-forward commands that result in the low frequency dynamic improvements.

Figure 4-3 is the closed loop response of the SVF controller showing a significant improvement in the low frequency response over the original data presented in Figure 4-1. We measured the frequency response using only the rate input to the command generator. The command generator creates the remaining elements of the command vector. We compute the transfer function between commanded position and measured position.

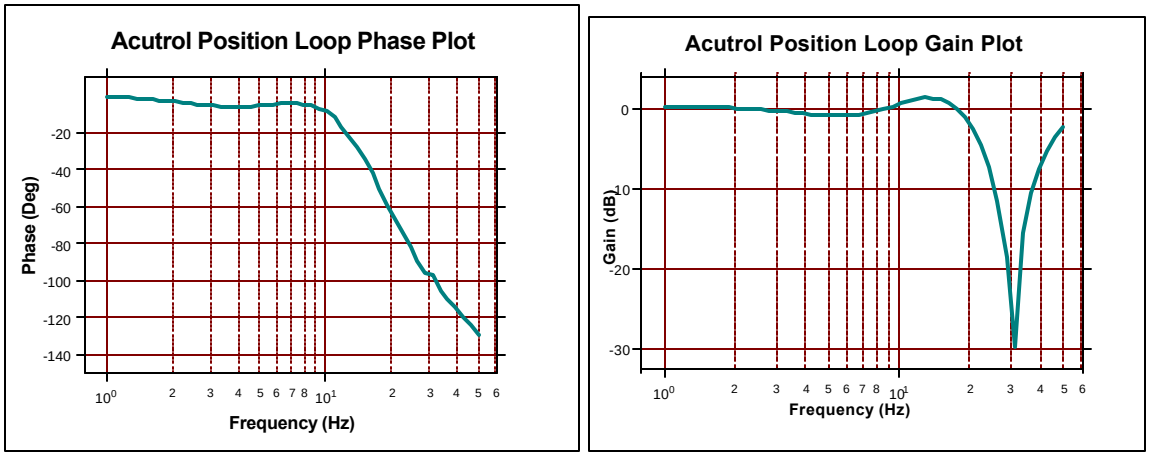

Figure 4-3 SVF Controller Outer Axis Closed Loop Frequency Response Showing a Phase Lag of only 9 Degrees at 10 Hz

The original axis controller has a phase lag of 28 degrees at 10 Hz while the SVF controller shows only a phase lag of 9 degrees at 10 Hz. The reduction in the phase lag will clearly enhance the ability of the HWIL simulation to approach the actual scenario. The phase lag reduction increases the flight table's transparency and simplifies the task of the autopilot designer to compensate for the flight table lag in the simulation.

During the demonstration we compensated the servo loop to produce wide stability margins in order to account for hydraulic plant variations and inertia load changes. We did this at the expense of the servo bandwidth (frequency at 90 degrees phase lag); which remained about the same as the original. Figure 4-4 demonstrates the stability margin system improvement with the SVF control system over the original controller. The figure shows the Nichols chart for both the original position controller and the SVF controller. We adjusted the closed loop response for the SVF controller by removing the feed-forward effects.

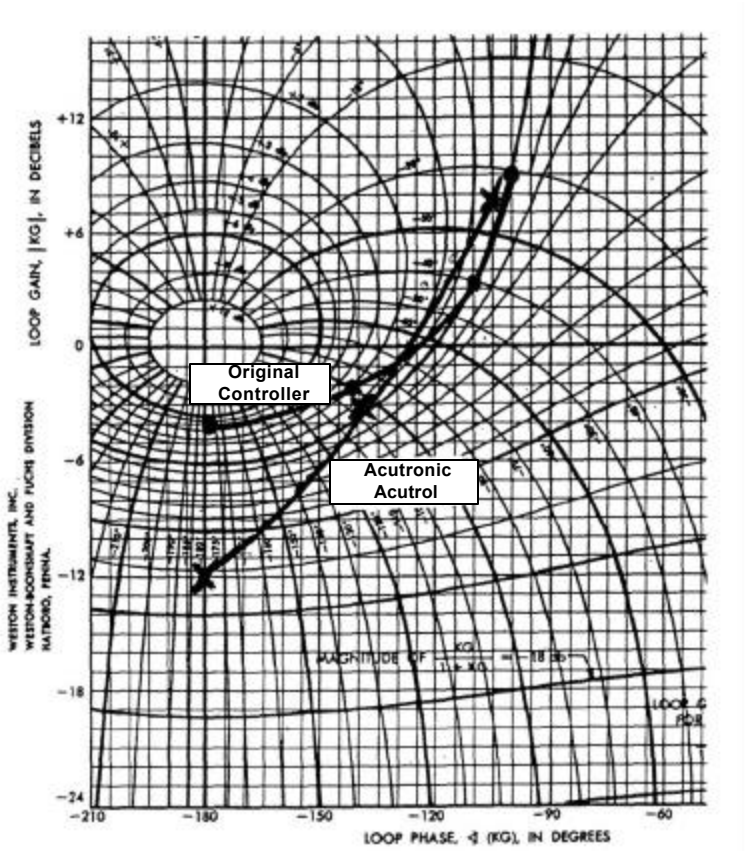

Figure 4-4 Nichols Chart Comparing the Original Control System with the SVF Controller and Showing over 8 dB Increase in Gain Margin

Figure 4-4 shows that the SVF controller has more than 8 dB (more than a factor of two) of gain margin increase over the original control system. The SVF control has a gain margin of 12dB compared to the 4dB gain margin of the original system. The low gain margin will significantly compromise the robustness of the axis control system. Variations in hydraulic properties over time and temperature and variations of the axis rotating inertia due to changes in the test article and gimbal orientations will seriously effect the servo stability. The original system's gain margin of only 4 dB was marginal and if the stability margins were increased then the system bandwidth would most likely have decreased.

Table 4-1 summarizes the overall improvement of the digital SVF controller over the original controller during the demonstration.

Table 4-1 Comparison of the Original to the Improved Axis Performance (with SVF Control)

Performance Criteria	Phase Lag @ 10 Hz, (Deg)	Mid Band Gain Variation, (dB)	Gain Margin, (dB)	Bandwidth (freq @ 90 deg), (Hz)
Original	29	-1 to +2	4	29
Improved	9	-1 to +1	12	29

4.2 Boeing Flight Table Modification

In the Boeing case we made permanent modifications to all three axes of the hydraulic flight table. We removed the existing control system and replaced it with the SVF digital Acutrol in a similar manner to the KHILS demonstration. Figures 4-5, 4-6 and 4-7 show the resulting closed loop frequency response (gain and phase lag vs. frequency) for the roll, pitch and yaw axes respectively. We measured the frequency response, as above, using only the rate input to the command generator. The command generator creates the remaining elements of the command vector. We then compute the transfer function between commanded position and measured position.

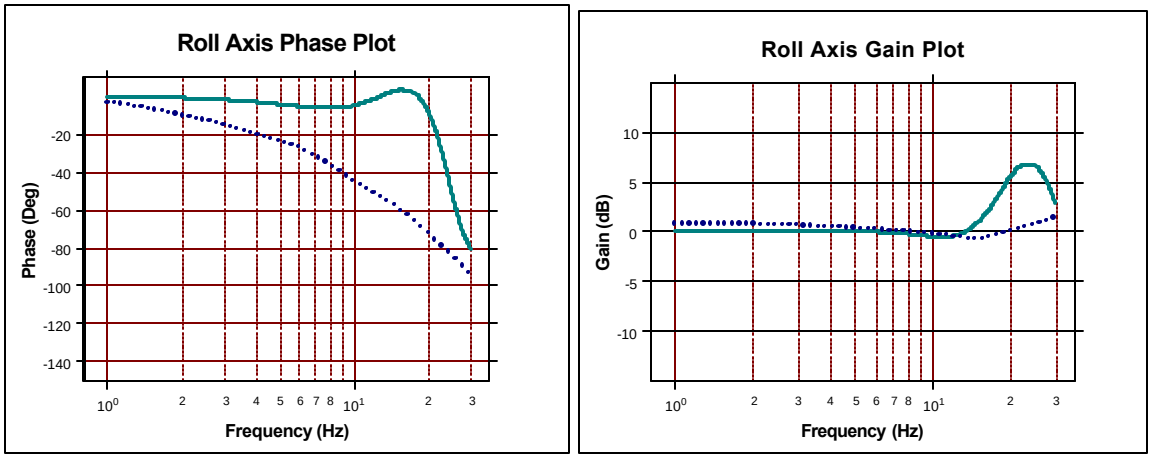

Figure 4-5 Roll Axis Closed Loop Frequency Response for SVF Controller (solid line) and Original Controller (dotted line) Showing a Phase Lag of only 5 Degrees at 10 Hz for the SVF Controller

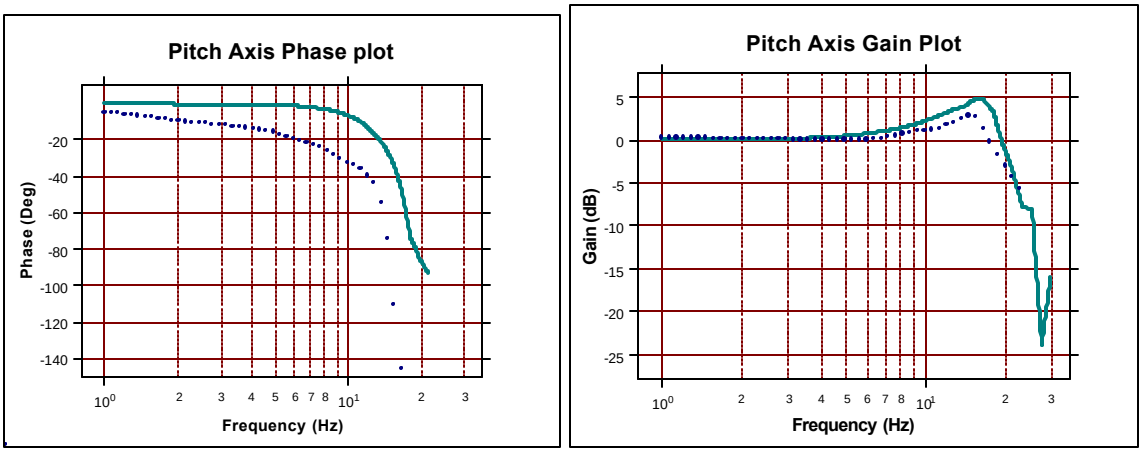

Figure 4-6 Pitch Axis Closed Loop Frequency Response for SVF Controller(solid line) and Original Controller (dotted line) Showing a Phase Lag of only 7 Degrees at 10 Hz for the SVF Controller

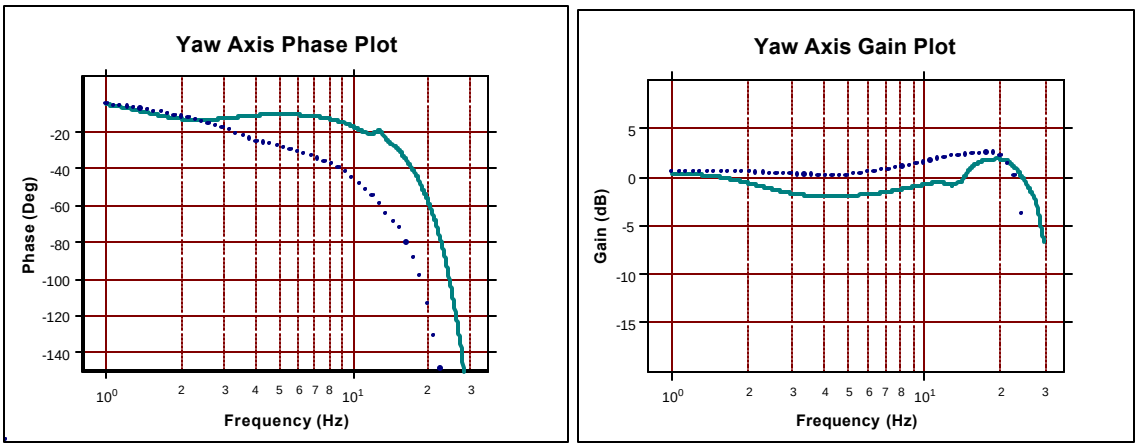

Figure 4-7 Yaw Axis Closed Loop Frequency Response for SVF Controller (solid line) and Original Controller (dotted line) Showing a Phase Lag of only 18 Degrees at 10 Hz for the SVF Controller

Table 4-2 summarizes the results of this case; here we compare previous data to the current data shown in figures 4-5, 4-6 and 4-7.

Table 4-2 Comparison of the Original to the Improved (SVF Control)

	Roll Axis		Pitch Axis		Yaw axis	
Performance Criteria	Original	Improved	Original	Improved	Original	Improved
Phase Lag @ 10 Hz (Deg)	40	5	35	7	45	18
Mid Band Gain Variation, (dB)	0 to 3.5	-0.5 to +6.5	0 to +3	0 to +5	0 to +2.5	-2 to +2
Bandwidth, Frequency at 90 deg phase lag (Hz.	29	>30	15	>20	18	24

Tables 4-1 and 4-2 show a significant reduction in the low frequency phase shift after we installed the digital SVF controller. We see reductions in closed loop phase lag ranging from a low of 20 degrees to a high of 35 degrees. The phase lag of the SVF controller ranges from a low of 5 degrees to a high of 18 degrees at 10 Hz. These values are representative of an 80 Hz., 0.7 damped second order system!

5. Summary

The results show that the implementation of the proper control system architecture will significantly reduce low frequency phase lag and thus increase the flight table dynamic transparency. The control system architecture contains a wide bandwidth pressure control sub-loop and uses feed-forward control techniques. These features provide:

- compensation for hydraulic resonance

- de-coupling of hydraulic dynamics from mechanical structural dynamics
- reduction of input/output phase response

Additionally, this controller increased the stability margin while maintaining or increasing servo bandwidth.

6. Acknowledgements

The authors wish to thank Lee Murrer for allowing us to perform this demonstration at the KHILS laboratory.

The authors also wish to thank Fred Wild and Gary Hart of the Boeing Company for giving us permission to present the data from the refurbishment of their flight table.

7. References

[1] TBD